MARS ATMOSPHERE RECONSTRUCTION USING A FLUSH AIR DATA SYSTEM ON THE EXOMARS ENTRY, DESCENT AND LANDING DEMONSTRATOR MODULE

Bart Van Hove[(1)], Özgür Karatekin[(2)]

[(1)] Royal Observatory of Belgium, Ringlaan 3, 1180 Brussel, Belgium, bart.vanhove@observatory.be

[(2)] ozgur.karatekin @observatory.be

ABSTRACT

On planetary exploration vehicles, FADS (Flush Air Data System) instrumentation to measure the entry flight environment is a novelty. The system performed successfully on Mars Science Laboratory (MSL). MSL is currently the only successful extra-terrestrial lander with a grid of surface pressure sensors integrated into the entry vehicle's heat shield. The 2016 ESA ExoMars demonstrator (EDM) will be the next planetary entry vehicle instrumented with FADS. In this study, a trajectory simulator was developed to generate synthetic flight data for ExoMars EDM. Subsequent reconstructions of the atmospheric environment using the simulated IMU (Inertial Measurement Unit) complementary FADS pressure flight data were evaluated in a preliminary uncertainty analysis. We found that along the 2016 ExoMars trajectory, neglecting high altitude atmospheric winds may result in significant bias error on density and derived atmospheric profiles. This error is significant for both atmospheric scenarios tested but particularly important in case of a global dust storm.

1 INTRODUCTION

Successfully landing vehicles on other planets is a challenging and rare performance. Accurately replicating entry conditions in ground test facilities is notoriously difficult. In this respect, Mars is the ultimate test facility for Mars entry. Therefore in-flight measurements must be fully exploited to gain knowledge on the vehicle's response to the planetary environment. Both the response and the atmospheric flight conditions must be reconstructed accurately to validate or improve ground predictions.

Reconstructions of past Mars entries have mainly relied on accelerations and angular rotations recorded by one or more IMU's (Inertial Measurement Unit). These allow for reconstruction of the flown trajectory as well as the highly variable atmospheric conditions on Mars. IMU flight data is well suited for trajectory reconstruction [1,2], but by itself may not suffice to accurately reconstruct the atmospheric environment. Variability of atmospheric conditions and in particular density has important implications for EDL mission design and performance. For example, the atmospheric density encountered by the Mars Exploration Rovers differed up to 12% from pre-flight predictions, which impacted the parachute firing altitude [3].

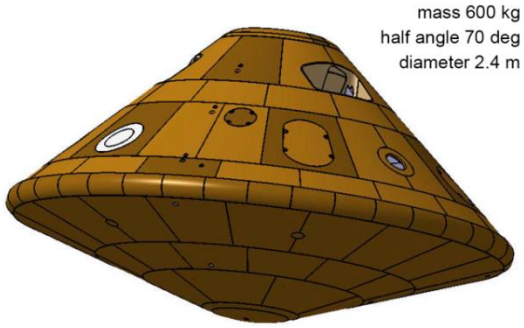

Fig. 1. Illustration of 2016 ESA ExoMars EDM [4]

It is beneficial for both mission performance and scientific investigation to improve understanding of the Martian atmosphere. Planetary entries provide in-situ information on atmospheric phenomena over a large altitude range compared to remote observations. Flush Air Data System (FADS) measurements are complementary to those by the IMU and, since the

FADS sensors are mounted on the vehicle's exterior, contain information about the atmospheric environment. This article describes methodology for reconstructing the atmospheric flight environment using both IMU and FADS (Flush Air Data System) heat shield surface pressure data.

1.1 Mission and spacecraft overview

NASA Mars Science Laboratory (MSL) was the first extra-terrestrial entry vehicle equipped with FADS. MSL landed on Mars in August 2012. ESA's ExoMars mission will fly a similar system through the Martian atmosphere in 2016. The ExoMars EDM (Entry, descent and landing Demonstrator Module) is the first of two ESA-Roscosmos Mars missions. In 2016, the Trace Gas Orbiter [5] and the EDM demonstrator, and in 2018 a larger Mars lander is scheduled. If successful, EDM will be Europe's first landing on the surface of Mars.

EDM will enter the Martian atmosphere at an altitude of 120 km with a velocity of about 6 km/s, from a location near the Equator. Solar longitude will be about 244° [6], which is in the Martian dust season characterized by highly variable weather and increased likelihood of global dust storms. ExoMars EDM and the similarly timed NASA InSight [7] will provide the first opportunities to observe Martian dust storms during entry.

The EDM entry vehicle design in Fig. 1 is similar to those of past successful Mars landers with a 70° half angle sphere-conical forebody. The back cone half angle measures 47° and the heat shield diameter is 2.4 m. More details on the shield design are given in [4]. The total entry mass of 600 kg includes the 300 kg surface platform [8]. The EDM aerodynamics are similar to those of Phoenix Mars Lander [9] and designed to produce a ballistic, zero trim angle trajectory. There is no thrust or active guidance during either high speed entry or the parachute descent phase.

1.2 Instrumentation

The EDM IMU sensor package contains multi-axis accelerometers and gyroscopes. By measuring translational accelerations and angular rotations at a sufficiently high frequency, the complete six degree of freedom (6-DOF) positional state of the vehicle can be derived. This involves numerical integration of the IMU signals, e.g. integrating acceleration over time to obtain vehicle velocity. 100 Hz is a sufficiently high sampling rate to allow for an accurate trajectory reconstruction.

IMU's are part of the standard instrumentation on planetary entry vehicles and measure the flown trajectory, i.e. where the vehicle is in a planet centered coordinate frame. However, IMU's are not exposed to the flow environment surrounding the vehicle. To gain insight into the atmospheric environment and the shock layer flow ahead of the heat shield, additional instrumentation could be useful.

Fig. 2. Instrumented engineering model of EDM heat shield [4]: arrows indicate flight pressure sensors

Similar to Mars Science Laboratory (MSL) [10], EDM is equipped with a grid of heat shield integrated thermal and pressure sensors. The latter correspond to the FADS that will be flown. The heat shield engineering model in Fig. 2 is equipped with more sensors than will be flown. The four surface pressure sensors that will actually be flown are marked by arrows. Three sensors are evenly spaced around a single sensor in the center. Since no time integration is required to interpret the pressures, they can be recorded at modest sampling rate of for example 10 Hz.

2 TRAJECTORY AND ATMOSPHERE RECONSTRUCTION USING IMU DATA

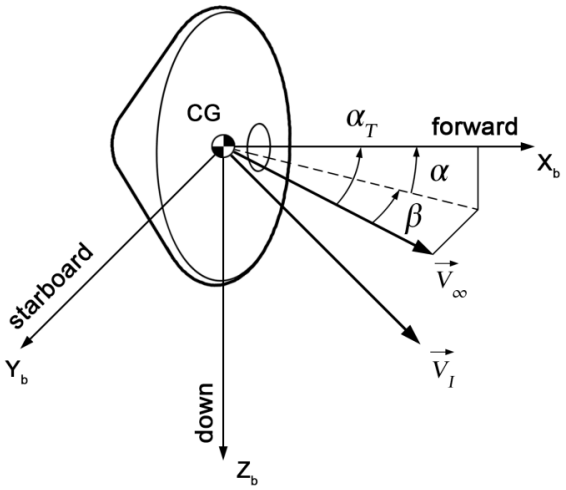

Fig. 3. Vehicle carried body frame with inertial and relative velocity vectors and flow angles

2.1 Trajectory reconstruction

Acceleration and angular velocity measurements have to be numerically integrated to provide the vehicle's positional state through time, i.e. its trajectory. The vehicle carries a body frame shown in Fig. 3, centered on the vehicle CG (center of gravity) and aligned with the vehicle geometry. Fig. 4 outlines an inertial planet centered frame: essentially it is the motion and position of the body frame in this inertial frame that is derived from IMU flight data.

Fig. 4 defines another common frame, carried by the vehicle CG but aligned with the local North, East and down directions. The NED frame is useful for specifying quantities with respect to a local horizontal surface (e.g. wind velocity) or expressing the trajectory (e.g. the flight path angle below local horizontal).

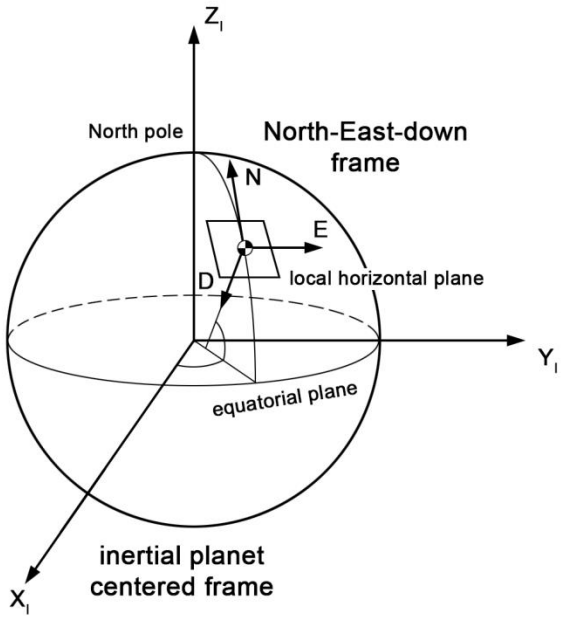

Fig. 4. Inertial frame centered on planet, NED frame centered on vehicle CG aligned with local horizontal

Fig. 3 defines two velocity vectors. $\vec{V}_I$ is the inertial velocity of the vehicle, measured relative to the inertial frame. On the other hand, relative velocity $\vec{V}_\infty$ is measured relative to the surrounding atmosphere and its magnitude gives the air speed. The direction of $\vec{V}_\infty$ is that of the oncoming flow, and is commonly expressed as angle of attack α and sideslip angle β, which can also be combined in a total angle of attack α_T.

$\vec{V}_I$ can be accurately derived from IMU data, which results from inertial measurements. In turn, $\vec{V}_\infty$ can be derived from $\vec{V}_I$. In Eq. 1 the cross product of vehicle position vector $\vec{R}_I$ and planet rotation vector $\vec{\omega}$ yields the atmosphere's rigid rotational velocity, and $\vec{V}_w$ is the wind velocity. These two terms represent atmospheric motion in the inertial frame, and are subtracted from $\vec{V}_I$ to obtain $\vec{V}_\infty$.

$$\vec{V}_\infty = \vec{V}_I - \vec{R}_I \times \vec{\omega} - \vec{V}_w \tag{1}$$

It is important to note that IMU flight data provides only $\vec{R}_I$ and $\vec{V}_I$ and that deriving $\vec{V}_\infty$ with Eq. 1 requires information on wind velocity $\vec{V}_w$. In high speed entry, wind velocity is usually small compared to inertial velocity, and $\vec{V}_w$ is commonly neglected.

In summary, by time integrating IMU signals an accurate trajectory in the inertial frame can be obtained. However, IMU's alone do not provide information on wind velocity which leads to an approximate relative velocity $\vec{V}_\infty$. This can affect the determination of air speed and flow angles as will be discussed below.

2.2 Atmosphere reconstruction

Given a trajectory from the IMU flight data, atmospheric density can be derived using the drag equation [11-14]. In Eq. 2, the drag equation has been rearranged to calculate atmospheric density ρ_∞ as a function of the vehicle's deceleration:

$$\rho_\infty(h) = 2\frac{m \cdot |\vec{a}|}{C_D \cdot A_{ref} \cdot |\vec{V}_\infty|^2} \tag{2}$$

$\rho_\infty(h)$ is the density profile versus altitude h, $|\vec{a}|$ the aerodynamic acceleration magnitude, C_D the non-dimensional aerodynamic drag coefficient, $|\vec{V}_\infty|$ the air speed, m the vehicle mass and A_{ref} the reference surface area based on the heat shield radius. Note that C_D is the *predicted* aerodynamic drag.

Other atmospheric profiles can be derived from the density profile in two steps. First, atmospheric pressure $p_\infty(h)$ is estimated by integrating density over altitude according to the hydrostatic equilibrium equation in Eq. 3. Second, density and pressure are combined in the ideal gas law to derive atmospheric temperature $T_\infty(h)$ in Eq. 4:

$$p_\infty(h) = p_\infty(h_0) - \int_{h_0}^{h} g \cdot \rho_\infty \cdot dh \tag{3}$$

$$T_\infty(h) = \frac{\mu \cdot p_\infty}{R \cdot \rho_\infty} \tag{4}$$

with gravitational acceleration g, ideal gas constant R = 8.3144621 J/mol/K and molecular weight μ of the atmospheric gas composition. μ and g vary slightly with altitude. Eq. 3 also requires a pressure boundary condition $p_\infty(h_0)$ that is often set to zero near the high

altitude entry interface, or specified at the surface if ground pressure measurements are available.

The main disadvantage of this IMU based atmosphere reconstruction method is the reliance of Eq. 2 on the aerodynamic drag coefficient. C_D estimations from pre-flight wind tunnel testing and/or CFD (computational fluid dynamics) cannot be compared against real-flight coefficients, because they serve as an input for the calculations. Furthermore, errors on predicted C_D are propagated to the atmospheric density and derived profiles. The 3-σ uncertainty bound on C_D for Mars entry vehicles like EDM, has been estimated at ±3% above Mach 10 and ±10% below Mach 5 in [9].

The reconstructed density in Eq. 2 also requires air speed $|\vec{V}_\infty|$. Since IMU flight data is insensitive to winds, an air speed estimated from Eq. 1 becomes an error source for atmosphere reconstruction, especially in the presence of strong winds.

3 ATMOSPHERE RECONSTRUCTION USING FADS

In recent decades, FADS has been developed for a variety of vehicles including jet fighters [15], the NASA Space Shuttle [16], sharp nosed hypersonic vehicles [17] and the future ESA Expert Earth re-entry testbed [18]. MSL is currently the only planetary exploration vehicle that flew FADS [19].

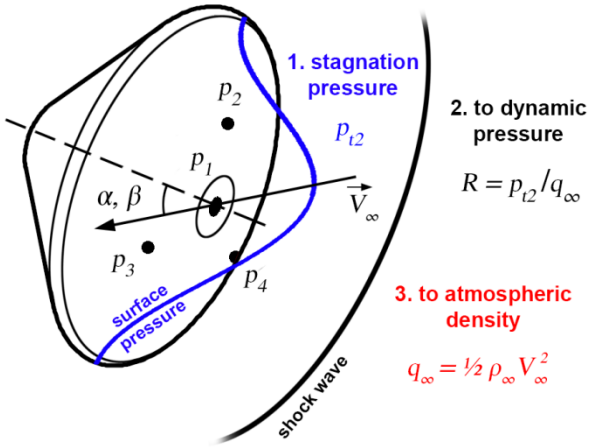

Fig. 5. Solution procedure of the FADS solver starting from (1), estimating stagnation pressure p_{t2} and flow angles α and β. Next (2) dynamic pressure q_∞ from pre-computed shock wave pressure ratio R and finally (3) atmospheric density ρ_∞ from q_∞ and air speed V_∞

The derivation of the flow environment from FADS pressure measurements is an inverse problem, as opposed to the more common forward calculation of the heat shield surface pressure distribution. Our FADS solver comprises three stages illustrated in Fig. 5: surface pressure distribution, dynamic pressure ahead of the shock wave and atmospheric density. Additional quantities solved for along the way include flow angles α, β, stagnation pressure p_{t2} and even atmospheric winds, although the latter is challenging at high speeds.

Potential benefits of flight reconstructions with FADS measurements include:

- No reliance on predicted aerodynamics.
- Flow angles derived from the observed flow field including winds.
- Improved air speed estimate if winds can be derived.

FADS reconstructed atmospheric density and derived atmospheric profiles do not rely on predictions of C_D. In fact, aerodynamic coefficients could be derived and compared to predictions. Deriving atmospheric winds from their impact on the flow angles, can potentially improve the air speed estimate and benefit density reconstruction further.

FADS sensors measure the pressure distribution on the heat shield surface. Solving the inverse problem requires a flow model. The flow model can be constructed using CFD [20], wind tunnel testing [15] or approximate analytical relations. Here, we used the latter to obtain a FADS solver that is generally applicable to a wide range of blunt nosed Mars entry vehicles.

3.1 Surface pressure model

For the present study we use the analytical modified Newtonian flow model described in Eq. 5. It predicts surface pressures based on flow momentum conservation normal to the surface [21]. Newtonian flow neglects mainly viscous boundary layer effects and shock wave stand-off distance and is a good approximation at hypersonic velocities.

$$p_i = (p_{t2} - p_\infty) \cdot \cos(\theta)^2 + p_\infty$$
$$\cos(\theta) = f(\alpha, \beta, \lambda_i, \phi_i) \qquad (5)$$

The surface pressure p_i is calculated as function of stagnation pressure p_{t2}, atmospheric pressure p_∞ and flow incidence angle θ. The θ angle measures the flow direction relative to the surface normal. It is calculated by a trigonometric function f which takes into account angles α and β representing flow direction, and cone and clock angles λ_i and ϕ_i that express the surface normal direction at the pressure port location. All these angles are defined with respect to the vehicle's symmetry axis.

Eq. 5 is inverted using a non-linear Newton solver. In principle p_{t2}, α, β and p_∞ can be derived using Eq. 5.

In practice, p_∞ is extremely difficult to estimate accurately since it is orders of magnitude smaller than the stagnation pressure p_{t2}, and the front pressure distribution on blunt vehicles is quite insensitive to p_∞. Conversely, this means that an independent p_∞ estimate, e.g. from IMU data (Section 2), can be provided as an input with negligible consequences for the FADS outputs. This is the approach we adopted.

3.2 Shock wave model

The pre-shock dynamic pressure $q_\infty = ½\,\rho_\infty V_\infty^2$ which is required for deriving density ρ_∞, is related to the post-shock conditions by the pressure ratio $R = p_{t2}/q_\infty$. An analytical approximation for R is the Rayleigh-pitot tube relation [16] given in Eq. 6:

$$R = \frac{2}{\gamma M_\infty^2}\left(\frac{(\gamma+1)^2 M_\infty^2}{4\gamma M_\infty^2 - 2(\gamma-1)}\right)^{\frac{\gamma}{\gamma-1}}\left(\frac{1-\gamma+2\gamma M_\infty^2}{\gamma+1}\right) \tag{6}$$

with Mach number M_∞ and the dimensionless ratio $\gamma = c_p/c_v$ of gas heat capacities at constant pressure and volume. Eq. 6 rests on the assumption that γ is constant through the shock. In reality, the temperature increase through a hypersonic shock wave affects gas properties significantly. Relations such as Eq. 6 describe *ideal* or *cold gas* behavior, while high temperature effects are sometimes referred to as *real gas* behavior.

To improve on Eq. 6, we constructed a database of pre-calculated pressure ratios R by numerically solving normal shock wave conservation equations of mass, energy and momentum. To include real gas effects, gas properties were provided by a high temperature thermodynamic library called Mutation developed at the von Karman Institute for Fluid Dynamics [22]. We calculated R in a suitable range of Mach numbers and atmospheric flight conditions for pure CO_2 gas. Future studies will use a more realistic Mars atmosphere composition including small amounts of N_2 and Ar.

Above Mach 5, we found that the impact of real gas effects on R exceeded 5%. It is worth mentioning that a similar real gas calculation for Earth entry [23] using high temperature air properties [24] found a similar discrepancy at high Mach numbers. This approach thus offers an important improvement over cold gas approximations while remaining generally applicable to a range of Mars entry vehicles.

3.3 Deriving atmospheric density and winds

Once the pre-shock stagnation pressure p_{t2} has been deteremind, the final stage of the FADS solver is the estimation of ρ_∞ from q_∞ according to Eq. 7:

$$\rho_\infty = 2\,q_\infty / V_\infty^2 \tag{7}$$

which also requires air speed. The V_∞ estimate of the IMU trajectory reconstruction can be used for this purpose, but since it is insensitive to atmospheric motion it does not take into account wind velocity.

Instead, it is possible to derive wind velocity from FADS measurements to improve the V_∞ estimate. Eqs. 8-10 relate the angle of attack α and sideslip angle β to the relative velocity vector $\vec{V}_\infty$ including the wind velocity vector $\vec{V}_w$ [25]. Recall that $\vec{R}_I \times \vec{\omega}$ represents rigid atmosphere rotation with the planet. In Eqs. 9-10 $\vec{V}_\infty$ is expressed in body frame coordinate components:

$$\vec{V}_\infty = \vec{V}_I - \vec{V}_w - \vec{R}_I \times \vec{\omega} \tag{8}$$

$$\alpha = \tan^{-1}\left(\vec{V}_\infty(z) \Big/ \vec{V}_\infty(x)\right) \tag{9}$$

$$\beta = \sin^{-1}\left(\vec{V}_\infty(y) \Big/ |\vec{V}_\infty|\right) \tag{10}$$

The FADS reconstructed values of α and β using Eq. 5 are in fact sensitive to winds. Substituting Eq. 8 in Eqs. 9-10 and neglecting vertical wind components, the system can be solved for $\vec{V}_w$ from α and β and thus yields a $\vec{V}_\infty$ estimate including horizontal wind components. Far above the planetary boundary layer, vertical winds are indeed negligible compared to horizontal winds. Note that the inertial velocity $\vec{V}_I$ is available from the IMU trajectory reconstruction.

The accuracy of the wind estimate is associated with those of the flow angle estimates. Since wind velocities are typically much smaller than the inertial velocity of an entry vehicle, their impact on the flow angles is relatively small. In case of a very poor FADS wind estimate, the zero wind IMU derived air speed may actually be more accurate.

4 ESA 2016 EXOMARS EDM CASE STUDY

We now apply the reconstruction tools described in Sections 2 and 3 to simulated flight data for the upcoming ExoMars EDM mission, including a Monte Carlo uncertainty analysis. The objective is to assess the sensitivity of atmospheric profile reconstruction to the approximations in IMU based reconstructions, as well as the potential of complementary FADS heat shield instrumentation for atmosphere reconstruction.

4.1 Trajectory and flight data simulation

ExoMars EDM is currently being developed by ESA. EDM will perform a ballistic entry: it has no propulsion and essentially plunges through the atmosphere with only gravitational and aerodynamic forces acting on it. In the present study we considered preliminary estimates of aerodynamic behavior and vehicle properties. We simulated the entry up to parachute opening, covering the entry phase from high altitude interface to around 5 km altitude using our in-house trajectory simulator. IMU and FADS synthetic flight data are used for the reconstruction of atmospheric profiles as described in Section 3.

The aerodynamics of EDM are similar to those of Mars Phoenix [9] due to its similar geometry. We specified aerodynamic forces, static moments and dynamic moments as a function of Knudsen number in the high altitude free molecular regime, and Mach number in the continuum flow regime. Vehicle geometry was described by the mass and heat shield diameter given in Section 1. Moments of rotational inertia were calculated assuming a homogeneous distribution of the 600 kg entry mass. This implies zero cross moments of inertia. The CG was positioned on the symmetry axis and 0.6 m behind the nose.

The flight simulator solves 6-DOF equations of motion [26] adapted to ballistic entry vehicles. This is done with a 4th order Runge Kutta numerical integrator. The initial vehicle state from which the simulator starts solving was specified at the Entry Interface Point (EIP). The EIP involves an altitude of about 120 km, air speed of about 6 km/s, zero pitch and yaw rates and initial roll rate of 18 deg/s. This EIP is lies in a launch window planned for ExoMars EDM [6].

Mars was described by an ellipsoid planet reference surface with a polar radius of 3376.20 km and equatorial radius of 3396.19 km reported in [27], which also specifies a Mars rotation rate of 7.088E-5 rad/s. The ellipsoid surface is used to align the local horizontal plane with, on which the NED (North-East-down) frame is based. Also geodetic altitude is measured normal to the ellipsoid. Gravity was modeled with a 2nd degree 0th order harmonic gravity model.

The atmospheric environment was specified by values extracted from the Mars Climate Database (MCD) [28] as vertical profiles at the time and location of the EIP. These include density, pressure, temperature, molecular weight, heat capacity ratio, dynamic viscosity and three-component winds, all varying with altitude. MCD is an inventory of high resolution LMD Mars Global Circulation Model (GCM) [29] solutions for several weather scenarios. We considered *normal* and *dust storm* scenarios. The latter describes heavy global dust storm conditions based on high dust opacity estimates from [30].

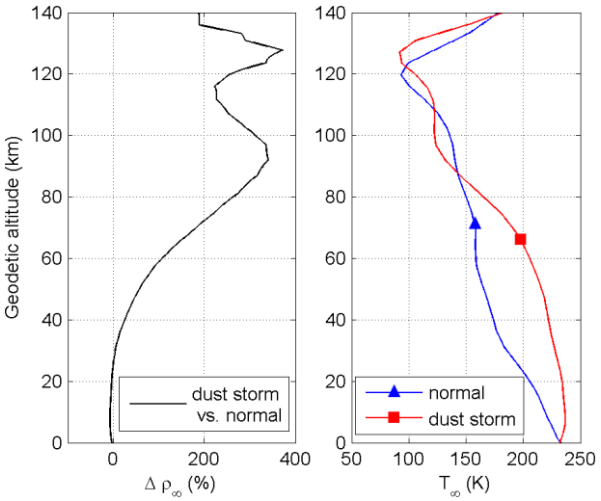

Fig. 6. MCD normal and dust storm scenarios: vertical profiles at EIP function of altitude

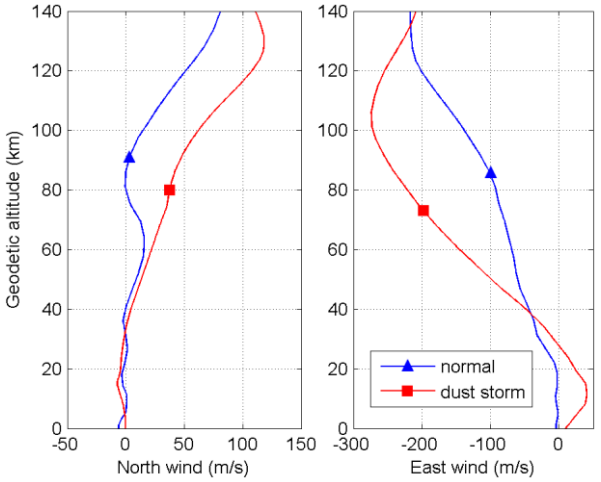

Fig. 7. MCD horizontal winds in normal and dust storm scenarios.

Fig. 6 shows considerable variation between the two weather scenarios. Above 70 km, density differs by over 200%. This does not however influence the vehicle trajectory much, since density at those altitudes is too low to produce significant aerodynamic drag. Fig. 7 compares horizontal wind profiles. Very fast westward winds are predicted, well exceeding 200 m/s above 80 km in the dust scenario. They are caused by migrating thermal tides rising from the sun lit surface and oppose the planet rotation at high altitudes. They are a feature of the sub solar equatorial or 'tropical' region of Mars. While they do not affect the trajectory much due to low atmospheric density, they can impact air speed according to Eq. 8.

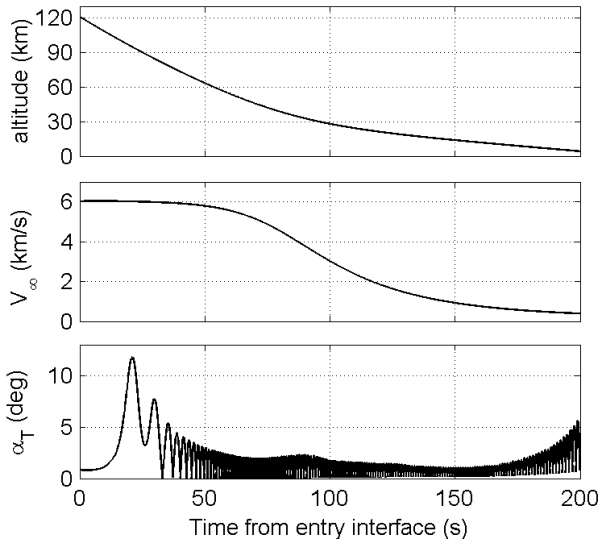

Fig. 8. Simulated ExoMars EDM trajectory (dust storm scenario)

The simulated EDM trajectory for the dust storm scenario is presented in Fig. 8. The trajectory for the normal weather scenario simulation is similar. The simulation was performed at a 20 ms time step (500 Hz) up to 200 s after EIP, when the conditions for parachute deployment were arrived at. The altitude and velocity decrease with time is similar to that of other Martian ballistic entries [12, 3]. During the critical events of peak deceleration (t ~ 100 s) and parachute opening conditions (t ! 200 s), total angle of attack is limited to 5°.

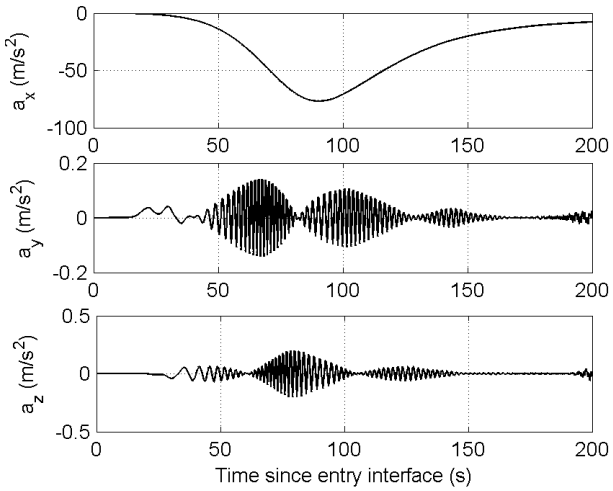

Fig. 9. Simulated body frame accelerations (dust storm scenario)

Fig. 9 shows the simulated IMU acceleration histories. This synthetic flight data is required for the subsequent reconstruction process. Peak acceleration occurs at about 30 km altitude and axial deceleration dominates.

Fig. 10 respectively shows the body roll, pitch and yaw rate histories. Since zero cross moments of inertia were specified, as well as zero roll damping and an on-axis CG location, the initial roll rate is maintained exactly. Peak pitch and yaw rates correspond closely to those obtained in an independent simulation [31].

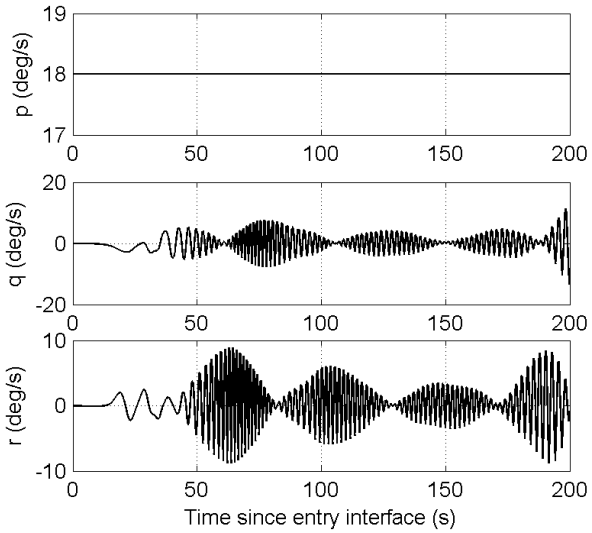

Fig. 10. Simulated body frame rotation rates: *p*, *q* and *r* components of total rotation vector (dust)

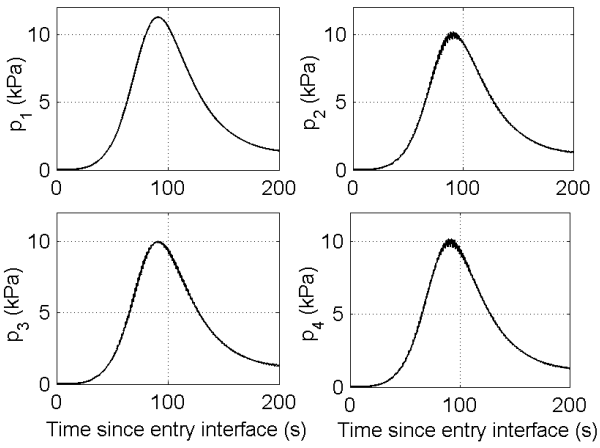

Fig. 11. Simulated FADS pressure signals (dust storm scenario)

FADS pressure signals were calculated from the flow angles, air speed and dynamic pressure using the approach described in Section 3. The resulting surface pressure histories at the four sensor locations on the EDM heat shield are given in Fig. 11. No signal noise has been added: but vehicle attitude oscillations are visible in the signals, especially for sensors p_2 and p_4.

4.2 Atmosphere reconstruction using IMU data

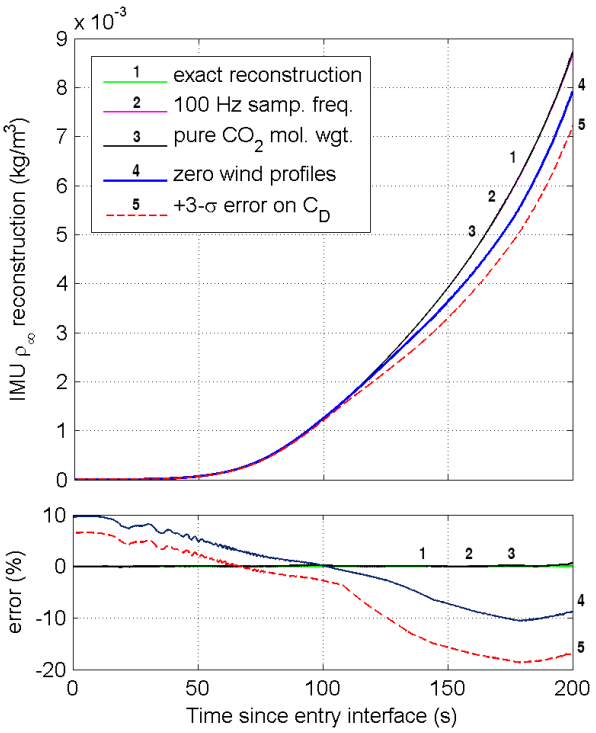

Fig. 12. Impact of approximations on IMU based atmospheric density reconstruction (dust storm scenario)

First, just IMU flight data is provided to the trajectory and atmosphere reconstruction routines, along with the exact simulator inputs including atmospheric winds. The resulting reconstruction matches the simulation results to numerical precision. Next, we proceed to progressively hide information from the reconstruction routine. This allows us to judge the impact of individual parameters and approximations in the reconstruction process, such as neglecting winds.

Fig. 12 shows the progressively accumulating impact of sampling frequency, molecular weight, atmospheric winds and aerodynamic drag coefficient C_D on reconstructed atmospheric density. Sampling IMU flight data at 100 Hz and assuming an atmosphere composed of pure CO_2 have negligible impact. Neglecting winds results in an error of up to 10%. The error sign depends on the direction of the wind profile. This is based on the GCM predictions for the global dust storm scenario. In the normal weather scenario, the wind speed would be lower (see Fig. 7) but still high enough to deteriorate atmosphere reconstruction by their exclusion from the IMU air speed estimate. This will be demonstrated below.

The dashed line in Fig. 12 represents the accumulated error due to all the approximations listed above, as well as a positive 3-σ adding error on C_D following [9]. This C_D error adds to or partially cancels with the previous errors, which are almost entirely due to neglecting winds. In summary, neglecting winds can affect atmospheric density reconstruction as significantly as mispredicting the drag coefficient.

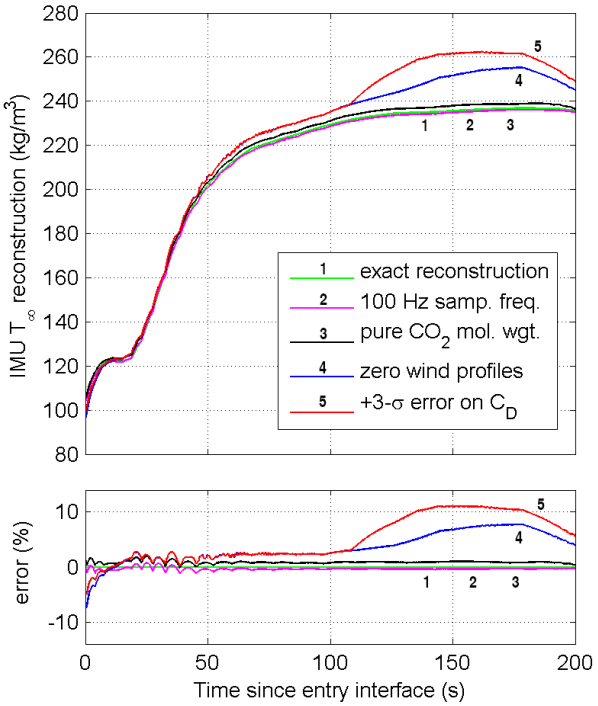

Fig. 13. Impact of approximations on IMU based atmospheric temperature reconstruction (dust storm scenario)

The impact of the above approximations on the reconstructed atmospheric pressure profile is very similar to that on the density profile, since pressure is obtained by numerically integrating density over altitude (Eq. 3). On the other hand, Fig. 13 shows that temperature profiles are affected less by assuming zero winds and mispredicting C_D, especially above 30 km altitude (before ~100 s). Temperature is obtained by dividing pressure through density in the ideal gas law (Eq. 4). The pure CO_2 assumption thus has a small but detectable impact on temperature where it had none on density. Below 30 km (after 100 s), total error still reaches 10%.

4.3 Atmosphere reconstruction using IMU and FADS data: Monte Carlo analysis

As shown in the previous section, the major errors in IMU data analysis are due to unknown atmospheric winds and uncertainties on the aerodynamic drag coefficient. In this section, we include the simulated FADS signals in the atmosphere reconstruction. We

assess the performance of IMU and IMU+FADS reconstruction methods with the help of Monte Carlo analysis. The synthetic flight data is provided by the simulations described above.

In the Monte Carlo analysis we performed one thousand reconstructions with stochastically normal distributed 3-σ errors on all the flight data and reconstruction inputs.

The assumed bias errors on the accelerometers and gyroscopes respectively were 0.3 milli-g and 1 °/hr. We further assumed white noise levels of 0.002 g/√Hz and 0.01 °/√Hz as well as scale factor errors of 350 ppm and 100 ppm for those instruments. For the FADS pressure sensors we considered noise errors of ±35 Pa and positioning errors of 1 mm. The shock wave pressure ratio database used by the FADS solver had a ±1% uncertainty associated with it, while the modified Newtonian flow model was assumed perfectly accurate. ±3-10% uncertainty [9] was associated with the drag coefficient C_D. EIP uncertainty estimates were based on those for Mars Phoenix lander [32]. Table 1 lists some additional 3-σ uncertainties.

	3-σ
vehicle mass	2 kg
initial atmospheric pressure	150 %
molecular weight	0.3 g/mol
heat capacity ratio	1.2 %

Table 1. Monte Carlo input uncertainties

The Monte Carlo analysis produces an ensemble of reconstruction outputs that can be compared to an ideal reconstruction, i.e. the original simulation. From the resulting output error ensembles, time histories of bias and standard deviation are calculated assuming a Gaussian distribution. We considered three reconstruction methods based on IMU data alone, and IMU+FADS data with or without attempting to derive atmospheric winds. IMU+FADS means trajectory reconstruction from IMU data and atmosphere reconstruction using the FADS solver described in Section 3.

In Fig. 14 the top plot shows the total uncertainty on reconstructed density, composed of output variance and the absolute value of average bias error. The bias error including its sign is shown separately in the bottom plot. Both IMU and IMU+FADS (zero wind) reconstructions have a cut-off altitude above which an accurate atmosphere reconstruction is infeasible, because both heat shield pressure and axial acceleration are too small to be measured with sufficient accuracy. This happens at 80 km in the FADS and 100 km in the IMU data.

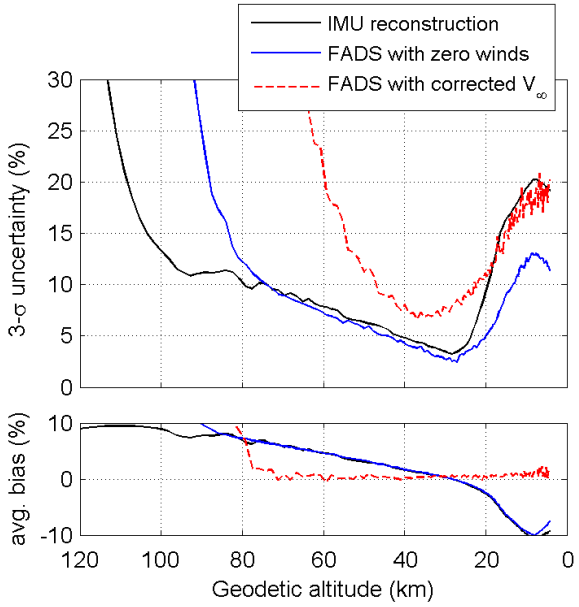

Fig. 14. Monte Carlo results for atmospheric density reconstruction (dust storm scenario)

Below 20 km, increased C_D uncertainty affects the IMU reconstruction, and decreased velocity lowers heat shield pressure closer to the pressure sensor accuracy limit. Nevertheless, IMU+FADS (with zero winds) compares favorably compared to IMU below 20 km.

The dashed line uncertainty in Fig. 14 represents the uncertainty on the IMU+FADS density profile derived using an air speed adjusted with FADS derived wind velocity. In the Monte Carlo output ensemble, the average bias error does indeed vanish below 80 km where the FADS measurements are most accurate. However, the wind estimate displays great variance and is actually detrimental to the air speed and atmosphere reconstructions. The total 3-σ bound on reconstructed density actually exceeds those obtained with a zero wind air speed estimate. In Fig. 15, the wind estimates with their 3-σ bounds show that the FADS sensors with the characteristics prescribed above, fail to constrain the winds.

Fig. 16 shows the total uncertainty on reconstructed density and temperature profiles for both global dust storm and normal weather scenarios. Only FADS using zero wind air speed is shown. Since winds are smaller in the normal weather scenario, the error associated with neglecting them is lower compared to the dust storm scenario. Nevertheless, the uncertainty is still significant for density, at about 5%. The temperature profiles were reconstructed from IMU data only, and are generally more accurate because common errors on pressure and density are divided out in the ideal gas equation (Eq. 4).

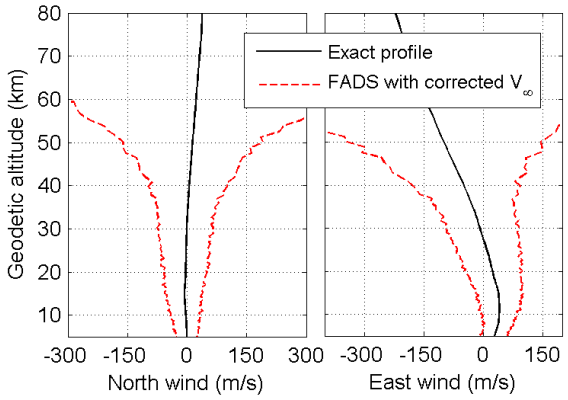

Fig. 15. Uncertainty on wind profiles reconstructed from FADS pressure measurements (dust storm scenario)

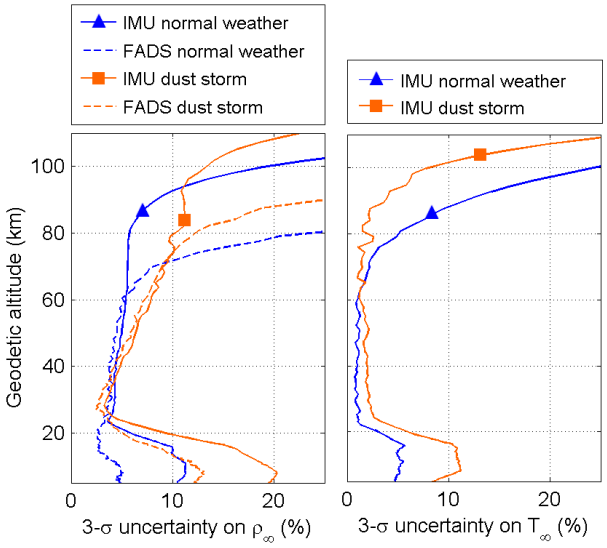

Fig. 16. Uncertainty on density and temperature profiles in normal and dust storm weather scenarios

5 CONCLUSION

We assessed the potential benefits of complementary FADS instrumentation in addition to IMU's for atmosphere reconstruction in a future post-flight analysis for ExoMars EDM 2016. The main advantages of FADS over IMU are no reliance on aerodynamic predictions and the possibility of observing winds to improve air speed estimates required for atmosphere reconstruction.

Given the assumed instrument uncertainties, atmospheric conditions and vehicle characteristics, we found that with either IMU or FADS, density can be reconstructed to better than 10% 3-σ uncertainty between 80 and 20 km altitude in a global dust storm scenario. For normal weather and in the same altitude range, this may improve to 5%. Depending on the weather scenario, these uncertainties are dominated by neglecting winds. This is a consequence of the high predicted winds and EDM's approximately equatorial flight path, increasing the sensitivity of air speed to those winds. According to GCM predictions, EDM could encounter westward winds at high altitudes, especially in a global dust storm.

Since EDM's FADS sensors are mainly installed for engineering purposes, it is perhaps unsurprising that their accuracy will be insufficient to observe atmospheric winds. The dependence of atmosphere reconstruction uncertainties on unknown wind velocity then remains. Regardless we found that below 20 km, FADS could improve atmosphere reconstruction compared to using IMU data exclusively.

REFERENCES

[1] P. N. Desai et al., Entry, Descent and Landing Performance of the Mars Phoenix Lander, J. of Spacecraft and Rockets, Vol. 48, No. 5, Sep-Oct (2011).

[2] D. W. Way et al., Assessment of the Mars Science Laboratory Entry, Descent, and Landing Simulation, 23rd AAS/AIAA Space Flight Mechanics Meeting, Kauai, HI on 10-14 February, (2013).

[3] P. N. Desai & P. C. Knocke, Mars Exploration Rovers Entry, Descent, and Landing Trajectory Analysis, J. of the Astronautical Sciences, Vol. 55, Issue 3, pp. 311-323, (2007).

[4] Y. Mignot et al., An insight into EXOMARS EDM HS development, ESA TPS Workshop 7th edition, ESA ESTECT, Noordwijk, The Netherlands on 8-10 April, (2013).

[5] M. Allen & O. Witasse, 2016 ESA/NASA ExoMars Trace Gas Orbiter, Mars Exploration Program Analysis Group (MEPAG), Lisbon, Portugal on June 16-17, (2011).

[6] L. V. Lorenzoni, ExoMars 2016 Entry Descent and Landing Demonstrator Module EDL overview, 10th International Planetary Probe Workshop, San Jose State University, CA on 17-21 June, (2013).

[7] W. B. Banerdt et al, InSight: A discovery mission to explore the interior of Mars, 44th Lunar and Planetary Science Conference, The Woodlands, TX on March 18-22, (2013).

[8] O. Bayle et al., ExoMars EDL Demonstrator Module (EDM) Mission and Design Overview, 8th International Planetary Probe Workshop, Portsmouth, VA on June 6-10, (2011).

[9] K. T. Edquist, P. N. Desai and M. Schoenenberger, Aerodynamics for Mars Phoenix Entry Capsule, J. of Spacecraft and Rockets 48 (5) (2011) 713–726.

[10] A. D. Steltzner et al., Mars Science Laboratory Entry, Descent and Landing System Overview,

AAS/AIAA 23rd Space Flight Mechanics Meeting, Kauai, HI in February, (2013).

[11] P. Withers et al., Analysis of entry accelerometer data: A case study of Mars Pathfinder, J. of Planetary and Space Science 51 (1) (2003) 541–561.

[12] R. C. Blanchard and P. N. Desai, Mars Phoenix Entry, Descent and Landing Trajectory and Atmosphere Reconstruction, J. of Spacecraft and Rockets 48 (5) (2011) 809–821.

[13] P. Withers and M. D. Smith, Atmospheric entry profiles from the Mars Exploration Rovers, Icarus 185 (1) (2006) 133–142.

[14] B. Kazeminejad, Methodology Development for the Reconstruction of the ESA Huygens Probe Entry and Descent Trajectory, Ph.D. thesis, Karl-Franzens University Graz, Institute for Physics, Austria (2005).

[15] B. R. Cobleigh et al., Flush Airdata Sensing (FADS) System Calibration Procedures and Results for Blunt Forebodies, NASA Technical Report TP-1999-209012 (1999).

[16] C. D. Pruett et al., Innovative Air Data System for the Space Shuttle Orbiter, J. of Spacecraft and Rockets, Vol. 20, No. 1, pp.61-69, (1983).

[17] M. C. Davis et al., Development of a Flush Airdata Sensing System on a Sharp-Nosed Vehicle for Flight at Mach 3 to 8, NASA TM-2000-209017, (2000).

[18] J. Häuser et al., Inverse Problem Solution for Determining Spacecraft Orientation from Pressure Measurements, 5th European Symposium on Aerothermodynamics for Space Vehicles (ESA SP-563), Cologne, Germany on 8-11 November, (2004).

[19] S. Dutta & R. D. Braun, Preliminary Statistical Trajectory and Atmosphere Reconstruction of MSL Entry, Descent and Landing, AAS-2013-309, (2013).

[20] I. A. Johnston, Simulation of Flow Around Hypersonic Blunt Nosed Vehicles for the Calibration of Air Data Systems, PhD thesis, University of Queensland, Dept. of Mechanical Engineering, (1999).

[21] J. D. Anderson, Fundamentals of Aerodynamics, McGraw-Hill Series in Aeronautical and Aerospace Engineering, (2005).

[22] T. E. Magin et al., Nonequilibrium radiative heat flux modelling for the Huygens entry probe, J. of Geophysical Research, Vol. 111, E07S12 (2006).

[23] P. zur Nieden & H. Olivier, Determination of Atmospheric Densities from Reentry Flight Data, J. of Spacecraft and Rockets, Vol. 44, No. 2, March-April (2007).

[24] S. Srinivasan et al., Simplified Curve Fits for the Thermodynamic Properties of Equilibrium Air, NASA RP-1181, (1987).

[25] C. D. Karlgaard et al., Mars Entry Atmospheric Data System Modelling and Algorithm Development, 41st AIAA Thermophysics Conference; San Antonio, TX; 22-25 Jun. 2009; United States, AIAA Conf. Paper 2009-3916; LF99-8954 (2009).

[26] R. F. Stengel, Flight Dynamics, Princeton University Press, ISBN 0-691-11407-2, (2004).

[27] P. K. Seidelmann et al., Report of the IAU-IAG Working Group on Cartographic Coordinates and Rotational Elements, Celestial Mechanics and Dynamical Astronomy, Vol. 98, pp. 155-180, (2007).

[28] Mars Climate Database v5.0, http://www-mars.lmd.jussieu.fr/ accessed in August 2013.

[29] F. Forget et al., Improved general circulation models of the Martian atmosphere from the surface to above 80 km, J. of Geophysical Research, Vol. 104, pp. 24, 155– 24,175, (1999).

[30] M. E. Ockert-Bell et al., Absorption and scattering properties of the Martian dust in the solar wavelengths, J. of Geophysical Research. Vol. 102, Iss. E4, pp. 9039-9050, 25 April, (1997).

[31] A. Aboudan et al., ExoMars 2016 Entry Probe Trajectory Simulation, 10th International Planetary Probe Workshop, San Jose State University, CA on 17-21 June, (2013).

[32] P. Withers & D. C. Catling, PHOENIX Atmospheric Structure Experiment (ASE) reduced data records (RDR), Planetary Data System (PDS), http://atmos.nmsu.edu/PDS/data/phxase_0002/ accessed in August 2013 (2010).